The Journal of Green Energy and Environmental Engineering

Research Paper

Mechanism of Antibiotic TC Degradation by H_2O_2

Paolo Paril[1,*], Tala Santangelo[1], Bela Carr[2]

[1] Consiglio per la ricerca in agricoltura e l'analisi dell'economia agraria, Centro di ricerca Ingegneria e Trasformazioni agroalimentari, Via della Pascolare 16, 00015, Monterotondo, Rome, Italy
[2] Bioproduct and Fiber Technology Team, AgResearch Limited, 1365 Springs Road, Lincoln, Christchurch, 7674, New Zealand
*Corresponding author: p.paril@crea.gov.it

Abstract. The mechanism by which EDTA-Fe^o catalyzes hydrogen peroxide (H_2O_2) to degrade pollutants remains unclear in alkaline-catalyzed H_2O_2 systems. This study selected EDTA-Fe^o as the catalyst and tetracycline (TC) as the target pollutant to investigate the degradation behavior and mechanism of the H_2O_2 system. The results demonstrated that the EDTA-FE^o/H_2O_2 system achieved 90.2% TC removal within 60 minutes under neutral conditions, whereas the unmodified FE^o/H_2O_2 system only removed 23.9% of TC. This modified FE^o broadened the pH limitations of Fenton-like reactions. The EDTA-FE^o/H_2O_2 system not only applied to various pollutants but also exhibited excellent recyclability, adaptability to natural substances, and effective performance in treating real wastewater. Using SEM, FTIR, XPS, WCA measurements, we confirmed the mechanisms by which EDTA-Fe^o efficiently catalyzed H_2O_2. Additionally, it was detected Fe–OH, Fe–OOH, and Fe–O peaks in both Fe^o hydrogen peroxide and EDTA-Fe^o hydrogen peroxide systems, proving that hydrogen peroxide decomposition follows two distinct pathways.

Keywords: *Tetracycline; Fe^0; Hydrogen Peroxide; Catalysis; Mechanism*

Received on 10 June 2024, Accepted on 20 August 2024, Published on 15 September 2024

1 Introduction

Tetracycline (TC) is an antibiotics, which is extensively found in the water environment, posing threats to ecosystems and human health [1]. Advanced oxidation processes (AOPs), including ozone oxidation, Fenton-oxidation, and photoelectrochemical oxidation, offer significant advantages for antibiotic treatment [2–6]. Among these, Fenton oxidation is widely applied industrially due to its simplicity and high efficiency. However, it suffers from high reagent consumption, secondary metal pollution, and pH limitations. Heterogeneous Fenton-like systems assisted by photo/electrochemical methods face challenges such as high energy input and catalyst recovery. Thus, developing a Fenton-like system that operates under alkaline conditions with low energy consumption, minimal secondary pollution, and high TC degradation efficiency is crucial for antibiotic pollution control.

H_2O_2-based systems have been successfully used to oxidize organic pollutants such as dyes [7–9], heavy metals [10], and chlorophenols [11]. In alkaline solutions, H_2O_2 decomposes to generate reactive species including hydroperoxyl anions (HO_2^-), hydroxyl radicals (HO•), superoxide radicals ($O_2•^-$), and singlet oxygen ($^1O_2$) [7, 12–16]. For example, HO_2^- was identified as the primary species in methylene blue degradation via N-demethylation and deamination [7], while $O_2•^-$ dominated in acid orange degradation [8]. Higher pH enhanced the degradation efficiency of rhodamine B, with HO• playing a key role [16].

Studies suggest that sodium bicarbonate ($NaHCO_3$) reacts with H_2O_2 to form peroxymonocarbonate (HCO_4^-), which decomposes into $CO_3•^-$, $^1O_2$, and $O_2•^-$ [18–19], differing from the mechanism of NaOH-catalyzed systems. For instance, $O_2•^-$ derived from HCO_4^- was the main active species in methylene blue degradation [15], rather

than HO_2^- [7]. Moreover, bicarbonate-catalyzed systems achieved higher degradation efficiency for acid orange at lower pH and with less oxidant [8, 20].

Thus, the oxidative performance of H_2O_2 systems depends not only on pH but also on the alkali catalyst type. This study examined TC degradation by H_2O_2 under various conditions and explored the mechanism using quenching experiments, electron paramagnetic resonance (EPR), and intermediate analysis.

2 Materials and Methods

2.1 Materials

UV-Vis spectrophotometer, pH meter, CO_2 cylinder, drying oven, thermostatic shaker, electronic balance were used in this work. Tetracycline hydrochloride (TC, ≥97%), Na_2HPO_4 (99%, Sigma-Aldrich Reagent Co.), $NaHCO_3$, Na_2CO_3, NaOH, HCl (36–38%), H_2O_2 (35%), tert-butanol (99%, Sigma-Aldrich Reagent Co.), furfuryl alcohol (98%), p-benzoquinone (AR, Aladdin Reagent Co.), CO_2 (99%, Sigma-Aldrich Reagent Co.).

2.2. Experimental Methods

A 30 mL TC solution was adjusted to pH 3.68–13.00 using 1 M NaOH, followed by H_2O_2 addition. Reactions were conducted in a shaking water-bath at 200 rpm, 25°C. Samples (0.4 mL) were periodically taken and quenched in 3.6 mL of 0.01 M HCl. TC concentration was measured, using a UV-Vis spectrophotometer, at 357 nm. All experiments in this work were run in duplicate.

2.3. Analytical Methods

TC-concentration was determined at 357 nm. The maximum absorption wavelength remained constant at 357 nm across pH values when samples were acidified.

Active species were detected using EPR (EPR200M). Intermediate products were analyzed via LC-MS (Thermo Q Exactive-Ultimate 3000 UPLC) with a C8 column, 50% methanol/water (0.1% formic acid) mobile phase, and ESI positive ion mode.

Kinetic analysis followed the pseudo-second-order model:

ct1−c01=kt

where c0and ctare initial and time-dependent concentrations (mg/L), tis time (min), and kis the rate constant (L/mg/min).

3 Results and Discussion

3.1 Performance of EDTA-FE^0/H2O2in degrading TC

According to the results shown in Figure 1a, under neutral conditions, the EDTA-FE^0/H_2O_2 system achieved a TC removal rate of 90.2% after 60 minutes of treatment. This performance was significantly higher than that of the EDTA-FE^0 system alone (30.3%), the FE^0/H_2O_2 system (23.9%), the FE^0 system alone (19.4%), and the H_2O_2 system alone (9.9%). This result demonstrates that EDTA-modified FE^0 enhances the removal efficiency of TC by H_2O_2 through catalytic oxidation [21].

The regeneration rate of Fe^{2+} seemingly determined the pollutant removal efficiency of the system [22]. Therefore, the concentration of Fe^{2+} was measured in the different systems. As shown in Figure 1b, at pH 6.5, the total iron concentration in the EDTA-FE^0/H_2O_2 system was 0.99 mg/L, comprising 0.24 mg/L of Fe^{2+} and 0.75 mg/L of Fe^{3+}. In contrast, the total iron concentration in the FE^0/H_2O_2 system under the same conditions was only 0.29 mg/L, comprising 0.05 mg/L of Fe^{2+} and 0.24 mg/L of Fe^{3+}. This indicates that EDTA-FE^0 can more

effectively activate H_2O_2 under neutral conditions [23], generating more Fe^{2+} and Fe^{3+}, thereby improving the reaction efficiency, whereas the reaction rate of the Fe^0 / H_2O_2 system is slower.

Reactive Oxygen Species (ROS) in the EDTA-Fe^0 / H_2O_2 and Fe^0 / hydrogen peroxide systems were measured in detail using Electron Paramagnetic Resonance (EPR) technology [24]. As shown in Figure 1c, the concentration of ·OH in the EDTA-FE^0/ hydrogen peroxide system was significantly higher than that in the Fe^0 / hydrogen peroxide system, reaching more than double the latter's concentration. This result highlights the crucial role of EDTA in promoting ·OH generation. Furthermore, within the first 20 minutes of the reaction, the ·OH concentration in the EDTA-FE^0/H_2O_2 system peaked at approximately 12 μM. This observation reveals the kinetic characteristics of hydroxyl radical generation in this system: in the beginning stage of the reaction, due to the efficient catalysis of EDTA-Fe^0 [25], hydroxyl radicals are generated rapidly. Subsequently, as the reaction proceeds, these radicals gradually participate in the degradation process of the pollutant, leading to a decrease in their concentration. This series of experimental results is consistent with previous studies, further validating the effectiveness of EDTA-FE^0 in promoting the decomposition of H_2O_2 to generate more ·OH [26]. These hydroxyl radicals are crucial for degrading the target pollutant, TC. Therefore, the EDTA-FE^0/H_2O_2 system demonstrates an enhanced ability to generate ·OH species under neutral conditions, leading to more effective degradation of organic pollutants [27].

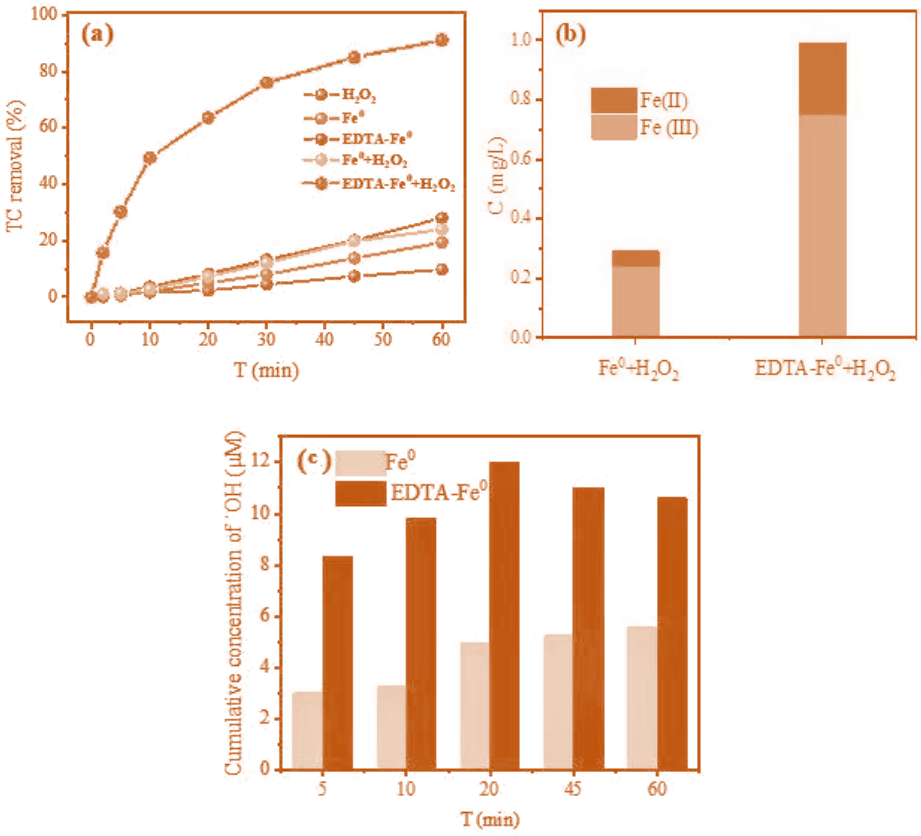

Figure 1 TC removal efficacy in the different oxidation systems (a); Fe^{2+} concentration and dissolved Fe^{3+} concentration in the different oxidation systems (b); cumulative concentrations of ·OH in the various oxidation systems (c)

To comprehensively evaluate the performance of EDTA-FE^0 in wastewater treatment, this study conducted a detailed comparison with other modified FE^0/H_2O_2 systems. The experimental results demonstrate that the EDTA-FE^0/H_2O_2 system exhibits significant advantages in TC removal.

As shown in Figure 2a, within a 60-minute reaction period, the EDTA-Fe^0/H_2O_2 system achieved a TC removal rate of 91.2%. This value is substantially higher than those of the oxalate-modified Fe^0/H_2O_2 system (79.6%),

borate-modified Fe^0/H_2O_2 system (59.2%), and phosphate-modified Fe^0/H_2O_2 system (30.9%). This comparative result indicates that EDTA-Fe^0 has a significant effect on enhancing the performance of the Fe^0 / hydrogen peroxide system compared to other modified Fe^0 systems, thereby achieving more efficient TC removal [28].

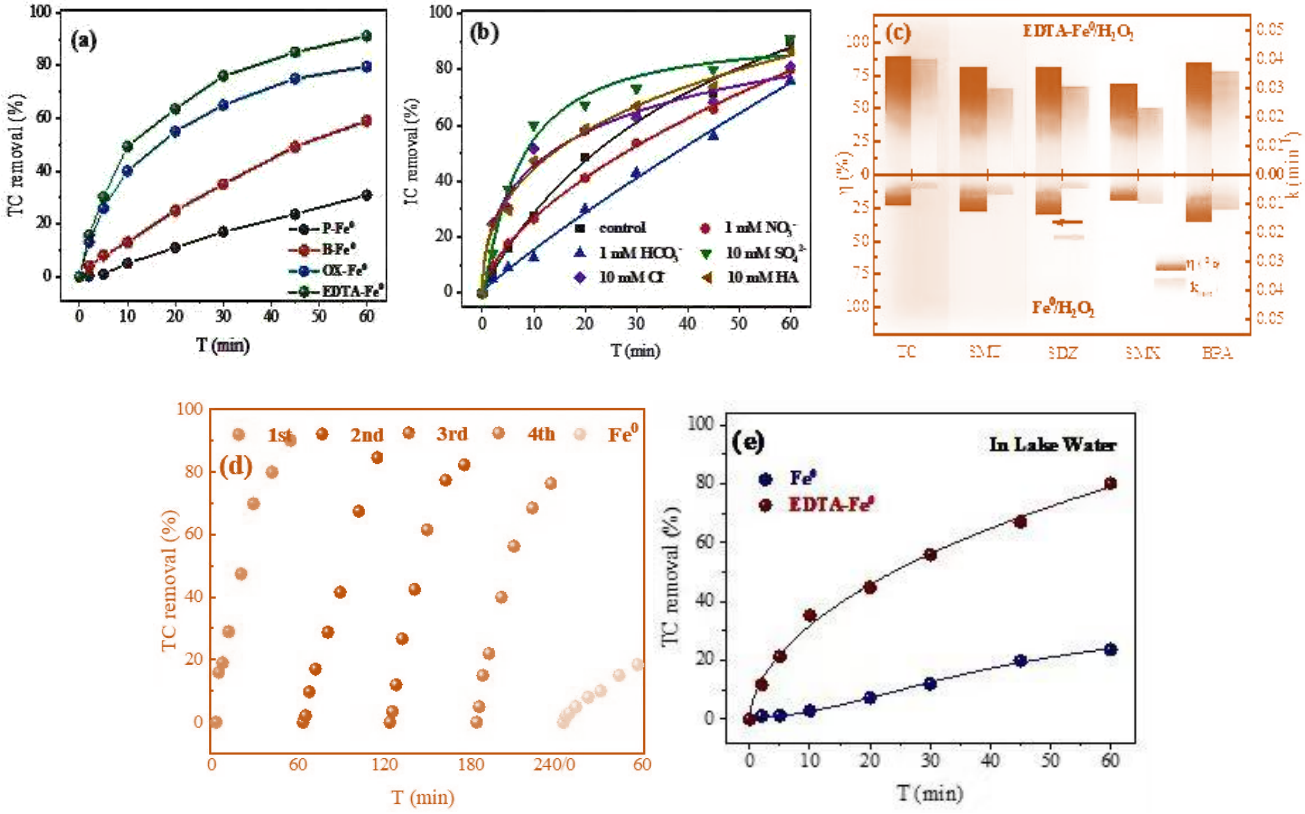

Figure 2 Removal efficacy of TC using various modified Fe^0 / hydrogen peroxide processes (a); influence of co-existing-inorganic-ions on TC removal in the EDTA-Fe^0 / hydrogen peroxide system (b); removal efficacies of various pollutants through the various oxidation systems (c); recyclability of EDTA-Fe^0 for TC removal in the EDTA-Fe^0 / hydrogen peroxide oxidation system (d); removal efficacy of TC in Tutem Lake water (e)

Figure 2b illustrates the practical application potential of the EDTA-FE^0/H_2O_2 system. Even in complex water environments containing various inorganic ions (such as Cl^-, NO_3^-, SO_4^{2-}, and HCO_3^-) and natural organic matter (e.g., Humic Acid, HA), the system maintained a TC removal rate above 75%. This result fully demonstrates the effectiveness and stability of the EDTA-Fe^0 / hydrogen peroxide system for treating actual wastewater.

Furthermore, the capability of the EDTA-Fe^0 / hydrogen peroxide system to treat different pollutants was evaluated. As depicted in Figure 2c, the removal rates for TC, SMX, SDZ, SMT, and BPA were 88.3% (k = 0.0396 min^{-1}), 80.9% (k = 0.0299 min^{-1}), 82.6% (k = 0.0301 min^{-1}), 67.4% (k = 0.023 min^{-1}), and 85.4% (k = 0.0357 min^{-1}), respectively. These values are significantly higher than those of the Fe^0 / hydrogen peroxide system: 23.6% (k = 0.0048 min^{-1}) and 28.9% (k = 0.0071 min^{-1}), among others. This indicates that the EDTA-F2^0 / hydrogen peroxide process enhances the removal capacity for various pollutants by 2.9 to 8.6 times compared to the Fe^0 / hydrogen peroxide process. This result further highlights the advantage of EDTA-Fe^0 in improving pollutant removal efficiency [29].

In terms of recyclability, EDTA-Fe^0 also demonstrated excellent performance. As shown in Figure 2d, after the fourth cycle, the removal rate of TC from the EDTA-Fe^0 / hydrogen peroxide system could still reach 76.3%, far exceeding that of the Fe^0 / hydrogen peroxide system (18.6%), proving its good stability.

Additionally, the EDTA-FE^0/H_2O_2 process was applied to treat actual water bodies. As shown in Figure 2e, when treating TC in water from Xuanwu Lake, the performance was similar to that in deionized water. This result not only verifies the practicality of the EDTA-FE^0/H_2O_2 process but also provides strong support for its application in real-world environments [30].

3.2 Study on the Mechanism of Enhanced H_2O_2 Activation by EDTA-Fe^0

3.2.1 Characterized Properties of EDTA-Fe^0

The surface chemical composition of Fe^0 and EDTA-Fe^0 system was thoroughly analysed using XPS, with the results illustrated in Figure 3a, Fig 3b. In the Fe 2p spectrum, a peak at a binding-energy of 705.9 eV was observed, which is attributed to Zero-Valent-Iron (FE^0, Fe^0). Additionally, peaks at binding-energies of 709.6 eV and 723.5 eV correspond to Fe^{2+} species. Compared to Fe^0, the proportion of Fe^{2+} in EDTA-Fe^0 increased significantly from 29.54% to 41.47%. This finding implied that EDTA modification enhances the reactivity of FE^0, which aligns with its high efficiency in pollutant degradation. Meanwhile, peaks observed at binding energies of 712.8 eV and 725.9 eV are assigned to Fe^{3+} species. In contrast to FE^0, the content of Fe^{3+} in EDTA-FE^0 decreased, which is associated with the increase in Fe^{2+} content. This further confirms that the introduction of EDTA alters the distribution of iron species on the FE^0 surface, potentially enhancing its activity in catalytic reactions. Figure 3b displays the O 1s spectra of FE^0 and EDTA-FE^0. Three distinct peaks are visible at binding energies of 528.9 eV, 530.6 eV, and 532.1 eV, corresponding to iron oxide, O-H groups, and H_2O, respectively. A comparison reveals a notable increase in the percentage of iron oxide in EDTA-FE^0. This result suggests that EDTA modification not only changes the distribution of iron species but also improves the iron oxide shell on the FE^0 surface. This improvement likely contributes to the enhanced stability and efficiency of EDTA-FE^0 in catalytic reactions. Based on the analysis results of XPS, it is hypothesized that an $Iron^{2+}$-rich oxide shell forms on the surface of EDTA-FE^0. This shell may play a critical role in the catalytic process by promoting electron transfer and reactant adsorption, thereby improving the performance of EDTA-FE^0 in wastewater treatment [31].

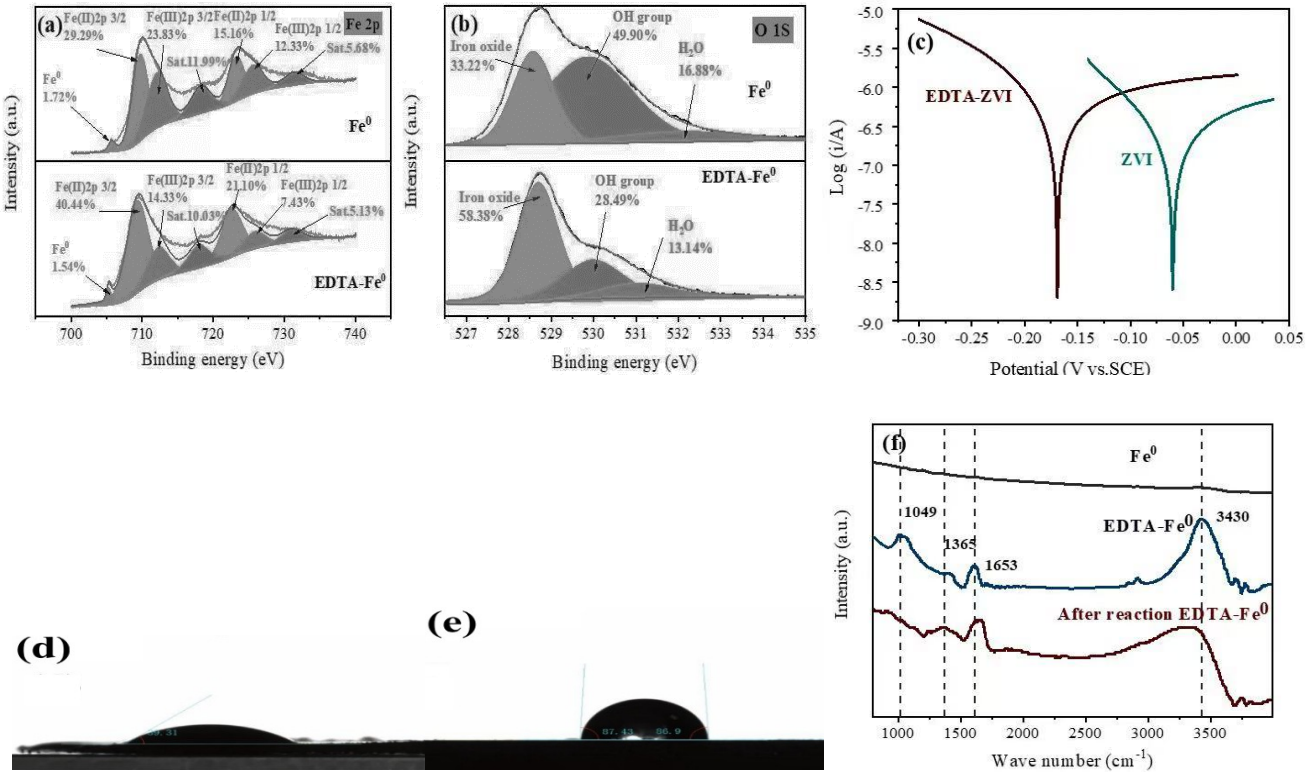

Figure 3 XPS analysis results of FE^0 and/or EDTA-FE^0; (a) Fe-2p; (b) O-1s; (c) Tafel analysis of FE^0 and EDTA-FE^0, WCA analysis of (d) FE^0 and (e) EDTA-FE^0 and (f) FTIR analysis of FE^0, EDTA-FE^0, and EDTA-FE^0 after the oxidation reaction

The results from the Tafel curves, shown in Figure 3c, further reveal differences in the electrochemical properties between EDTA-FE^0 and FE^0. Specifically, the corrosion potential of EDTA-FE^0 is -0.168 V, which is notably lower than that of FE^0 (-0.041 V). The corrosion potential is a key indicator of a material's tendency to corrode; a lower corrosion potential generally implies a greater propensity for electron transfer and corrosion. Therefore, this result indicates that EDTA-FE^0 possesses higher reactivity compared to FE^0, facilitating easier electron release during catalysis and thereby promoting pollutant degradation [32].

Furthermore, as shown in Figures 3d and 3e, the introduction of EDTA significantly altered the contact angle of FE^0. The static-water-contact-angle (SWCA) is an important factor for determining the wettability of the surface of a material. A lower static WCA indicates a better hydrophilicity, while a larger contact angle suggests stronger hydrophobicity. After EDTA modification, the contact angle of FE^0 increased markedly from 39.31° to 87.16°, indicating that EDTA-FE^0 exhibits enhanced hydrophobicity. This hydrophobic property is significant in wastewater treatment for two main reasons: Firstly, superior hydrophobicity effectively repels water molecules, reducing their contact with the material surface and minimizing the likelihood of surface occupation by water. Secondly, reduced water contact helps prevent passivation. Consequently, the strong hydrophobicity of EDTA-FE^0 aids in maintaining its catalytic activity and improves the efficacy of water treatment [33].

The coordination mode, on the FE^0 surface, was clarified, using Attenuated Total Reflectance (ATR) based Fourier-Transform-Infrared-Spectroscopy (ATR-FTIR), for semi-quantification. As shown in Figure 3f, peaks that found at 1655 cm^{-1} as well as 1369 cm^{-1} are mainly resulted from the vibration of asymmetric-stretching and vibration of symmetric-stretching of carboxyl group (-COOH), respectively, indicating presence of carboxyl (COOH) groups on surface of EDTA-FE^0 material. A Δv value that was 200 cm^{-1} higher indicated monodentate coordination between EDTA and FE^0, potentially generating an either monodentate inner-sphere complex which was directly coordinated to metal ions on material surface. Or, it implied an outer-sphere complex, which was coordinated via only single EDTA-COO group and an -O=O-C bond. Compared to pure EDTA (1611 cm^{-1}), the -COO- peak that from EDTA-FE^0 material turned to a greater wavenumber, indicating that, the oxygen of carboxyl groups form direct linkages with Fe on material surface. This interaction reduced length of C=O linkage, while increasing the frequency of -COO- vibration, giving rise to a peak at a higher wavenumber. Therefore, adsorption of EDTA to the FE^0 materials surface is characterized as monodentate inner-sphere binding. EDTA adsorbs onto the FE^0 surface via oxygen atoms from its carboxyl groups, while the residual NH2 and COOH groups extend from material surface. This modified structure improves the shell of iron oxide on FE^0 material surface, delaying passivation of iron, while maintaining the EDTA-FE^0 material activity during oxidation reactions. As results, interactions of EDTA and FE^0 materials modified the environment, especially chemically, of irons, thereby influencing the cleavage of H_2O_2 [34]. Thus, the ATR-FTIR results also confirm the successful adsorption/reaction of EDTA onto FE^0 material surface.

3.2.2 Mechanism of H_2O_2 Activation in the Oxidation System based on EDTA-FE^0/H_2O_2

Previous research indicates that the decomposition of H_2O_2 involves the cleavage of the Oxygen–Oxygen bond, resulting in the generation of hydroxyl radicals (·OH, Equation 1). Furthermore, in the presence of a catalyst, H_2O_2 can also undergo O–H bond cleavage to produce *OOH species, which can further generate ·OH radicals via Equation (2). Detecting the *OOH species is crucial for confirming the reaction described in Equation (2). The Shell-Isolated Enhanced Nanoparticle-Raman Spectroscopy (SHINERS) technique, capable of enhancing signals from species that adsorbed to the surface of catalyst, by a factor of 10^7 to 10^9, was employed to detect *OOH [35].

According to the results presented in Figure 4a, the illustrated spectrum of the EDTA-FE^0 oxidation system alone (without H_2O_2) after reaction showed no distinct peaks. In contrast, both the EDTA-FE^0/H_2O_2 and FE^0/H_2O_2 oxidation systems showed three different distinct peaks after oxidation reaction [36]. These different peaks, located at 564 cm^{-1}, 634 cm^{-1}, and 1096 cm^{-1}, are assigned to the stretching-vibration of Fe–OH species, the stretching-vibration of Fe–OOH species, as well as Fe–O_2^- species [148], respectively. The existance of the peak at 634 cm^{-1} confirms the formation of *OOH species during the catalytic oxidative decomposition of H_2O_2 in both the EDTA-FE^0 / hydrogen peroxide and FE^0 / hydrogen peroxide oxidation systems.

Notably, the peak intensitiesin the EDTA-FE^0 / hydrogen peroxide system were higher thanin the FE^0 / hydrogen peroxide system, indicating a higher degree of formation of *OOH species in the EDTA-FE^0 / hydrogen peroxide system. This demonstrates that the enhancing effect of EDTA promotes the generation of *OOH species during the catalytic decomposition of H_2O_2. This result further corroborates the mechanism of enhanced ·OH radical production in the EDTA-FE^0 / hydrogen peroxide system and deepens our understanding of the overall reaction mechanism [35].

Based on the SHINERS spectra, the coexistence of both pathways (Equation 1 and Equation 2) in the EDTA-FE^0/H_2O_2 system was confirmed. To further investigate the relative importance of these different H_2O_2 decomposition pathways in the actual reaction, in-depth simulations and analyses were conducted using Density Functional Theory (DFT) calculations.

As shown in Figure 4b, in Path I, H_2O_2 is stably adsorbed on two Fe species via a dual Fe–O-coordination mode. This adsorption promotes the conversion of hydrogen peroxide-to-OH accompanied by the break of the peroxide bond. This pathway is in line with the widely reported traditional mechanism. However, as illustrated in Figure 4c, in Path II, H_2O_2 interacts with only one iron atom via a single-step Fe–O-coordination, leading to the formation of an *OOH (Fe–O–OH) intermediate through O–H bond cleavage [34]. Subsequent cleavage of the peroxide bond generates ·OH or OH^-. The proposal of this pathway enriches the understanding of the mechanism by which EDTA-FE^0 catalyzes hydrogen peroxide. However, as illustrated in Figure 4c, Path II involves H_2O_2 interacting with a single iron atom through a monodentate Fe–Ocoordination. This interaction leads to the formation of an *OOH intermediate (Fe–O–OH) via O–Hbondcleavage. Subsequently, the cleavage of the peroxide bond generates OH^- or ·OH. The proposal of this pathway enriches the understanding of the catalytic mechanism of hydrogen peroxide by EDTA-FE^0. The DFT calculation results revealed that the Gibbs free energy for the formation of HO–OH during hydrogen peroxide decomposition by EDTA-FE^0 is lower than that for the formation of H–OOH. This implies that the generation of HO–OH is more thermodynamically favorable and thus more likely to occur under actual reaction conditions. Through the comprehensive analysis of SHINERS spectra and DFT calculations, the different decomposition pathways of hydrogen peroxide in the EDTA-FE^0 / hydrogen peroxide system were thoroughly investigated. These findings not only deepen the understanding of the entire reaction mechanism but also provide an important theoretical basis for the optimization and broader application of EDTA-FE^0 [35].

$$* H_2O_2 \rightarrow * OH - OH(TS) \rightarrow * OH \rightarrow \cdot OH \quad (1)$$

$$* H_2O_2 \rightarrow * H - OOH(TS) \rightarrow * OOH \rightarrow \cdot OH \quad (2)$$

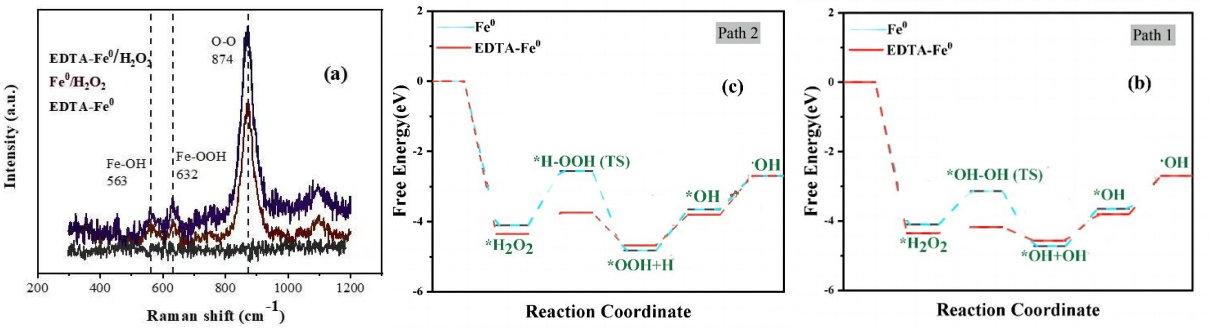

Figure 4 SHINERS spectrum of FE^0/H2O2 and EDTA-FE^0/H2O2

3.3 Formation of Intermediate Byproducts and Cytotoxicity

To clarify the degradation mechanisms of TC, intermediates generated in the EDTA-FE^0 / hydrogen peroxide system were identified using LC-MS. Based on the detected intermediates, a degradation pathway for TC was proposed. Pathway 1: Cleavage of the N–C bond in TC occurs due to its relatively low bond energy, facilitating demethylation to form TC4. Subsequent steps involving dehydroxylation, carbon-bond cleavage, and oxidation

convert TC4 into TC6 and TC7. Pathway 2: TC1 and TC8 are generated through complex processes, including cleavage of carbon (C)=carbon (C) double bonds and rearrangement of hydroxyl radicals at carbon 5. A key step is the oxidation of the N-methyl group to an N-aldehyde group, altering the molecule's chemical structure and bioactivity. Pathway 3: Separation of the amide group in TC leads to TC2 formation, followed by ring cleavage of carbon ring A to produce TC3. TC5 is formed via dehydration, deamination, and hydroxyl removal at carbon 11. In all pathways, intermediates are ultimately oxidized into harmless CO_2 and H_2O. In summary, intermediates formed during TC degradation in the EDTA-FE^0 / hydrogen peroxide system effectively reduce overall toxicity levels. These findings not only clarify the degradation pathway but also highlight the environmental benefits and low-toxicity advantages of the EDTA-FE^0 / hydrogen peroxide system.

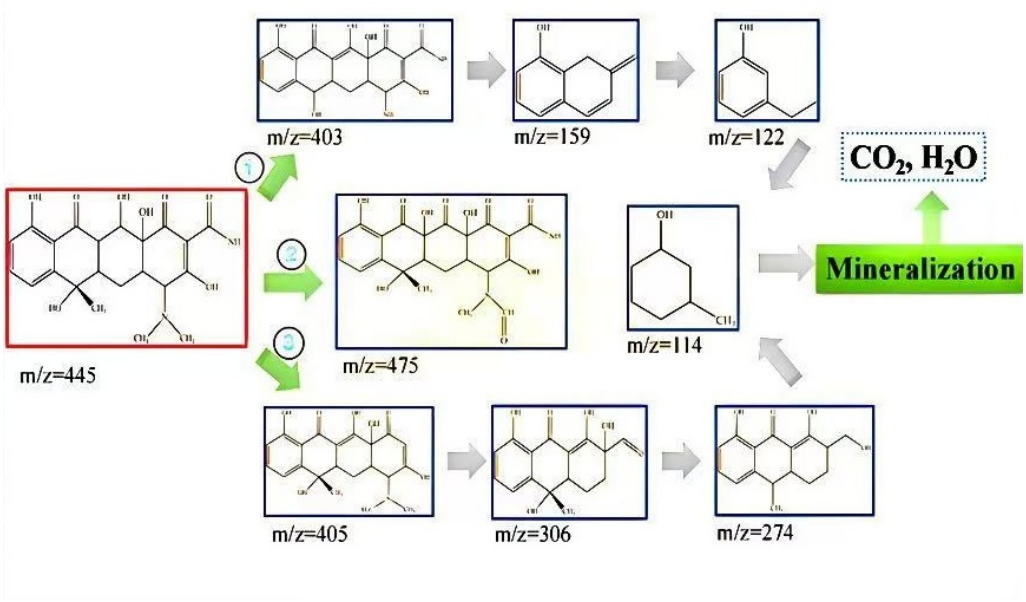

Figure 5 Possible pathways for TC degradation in the EDTA-FE^0/H2O2 system

4 Conclusions

The EDTA-FE^0/H_2O_2 system achieved 90.2% TC removal within 60 minutes under neutral conditions, significantly outperforming the unmodified FE^0/H_2O_2 system (23.9% removal). This modified FE^0 effectively

The EDTA-FE^0/H_2O_2 system not only exhibits applicability to diverse pollutants but also possesses excellent recyclability and adaptability to natural substances. Moreover, it demonstrates robust performance in treating actual wastewater.

Through characterization techniques including SEM, FTIR, XPS, WCA, we clarify the mechanismx by which EDTA-FE^0 effectively catalyzes hydrogen peroxide. Additionally, SHINERS analysis detected Fe–OH, Fe–OOH, and Fe–O peaks in both the EDTA-FE^0 / hydrogen peroxide and FE^0 / hydrogen peroxide systems, confirming that hydrogen peroxide decomposition proceeds via two distinct pathways during the reaction.

These findings collectively highlight the enhanced efficiency, versatility, and mechanistic insights provided by the EDTA-FE^0 modification, establishing its potential for practical environmental applications.

References

[1] Zhu Y, Li H, Zhang G, et al. Removal of hexavalent chromium from aqueous solution by different surface-m odified biochars: Acid washing, nanoscale zero-valent iron and ferric iron loading [J]. Bioresource Technol ogy, 2018, 261: 142-50.

[2] Liang Y, Min X, Chai L, et al. Stabilization of arsenic sludge with mechanochemically modified zero valent i ron [J]. Chemosphere, 2017, 168: 1142-51.
[3] Huang X, Chen P, Shi J, et al. Natural substance-mediated synthesis for biochar-supported nanoscale zero-valent iron enhanced the performance of the catalytic process [J]. Materials Today Sustainability, 2023, 2 3: 100461
[4] Biswal B K, Balasubramanian R. Adsorptive removal of sulfonamides, tetracyclines and quinolones from w astewater and water using carbon-based materials: recent developments and future directions[J]. Journal of Cleaner Production, 2022, 349: 131421.
[5] Huang T, Zhang G, Zhang N, et al. Pre-magnetization by weak magnetic field enhancing Fe0-Fenton proces s for wastewater treatment [J]. Chemical Engineering Journal, 2018, 346: 120-6.
[6] Van Gijn K, Zhao Y, Balasubramaniam A, et al. The effect of organic matter fractions on micropollutant oz onation in wastewater effluents[J]. Water Research, 2022, 222: 118933.
[7] Wu Y, Zhu J-y, Bai J-w, et al. The ability of pre-magnetized zero-valent iron for peroxymonosulfate activati on to remove ofloxacin [J]. Chemical Engineering Journal, 2023, 461: 141825.
[8] Gorito A M, Ribeiro A R L, Rodrigues P, et al. Antibiotics removal from aquaculture effluents by ozonation: chemical and toxicity descriptors[J]. Water Research, 2022, 218: 118497.
[9] Zhang Y, Zhou M. A critical review of the application of chelating agents to enable Fenton and Fenton-like reactions at high pH values [J]. Journal of Hazardous Materials, 2019, 362: 436-50.
[10] Vadakke Pariyarath R, Inagaki Y, Sakakibara Y. Phycoremediation of tetracycline via bio-Fenton process us ing diatoms[J]. Journal of Water Process Engineering, 2021, 40: 101851.
[11] Liu M, Ye Y, Xu L, et al. Recent Advances in Nanoscale Zero-Valent Iron (nZVI)-Based Advanced Oxidation Processes (AOPs): Applications, Mechanisms, and Future Prospects [J]. Nanomaterials, 2023, 13(21): 283 0.
[12] Bounab N, Duclaux L, Reinert L, et al. Improvement of zero valent iron nanoparticles by ultrasound-assiste d synthesis, study of Cr(VI) removal and application for the treatment of metal surface processing wastew ater [J]. Journal of Environmental Chemical Engineering, 2021, 9(1): 104773.
[13] Liao M, Wang X, Cao S, et al. Oxalate Modification Dramatically Promoted Cr(VI) Removal with Zero-Valen t Iron [J]. ACS ES&T Water, 2021, 1(9): 2109-18.
[14] Li Y H, Zhang Q F, Lu Y, et al. Surface hydroxylation of TiO2/g- C3N4 photocatalyst for photo-Fenton degra dation of tetracycline [J]. Ceramics International, 2022, 48(1): 1306-1313.
[15] Karthick A, Roy B, Chattopadhyay P. Comparison of zero-valent iron and iron oxide nanoparticle stabilized alkyl polyglucoside phosphate foams for remediation of diesel-contaminated soils [J]. Journal of Environ mental Management, 2019, 240: 93-107.
[16] Meng X X, Liu Z, Qian X B, et al. Enhanced degradation mechanism of anticancer drug irinotecan through l ow-frequency ultrasound assisted reactive electrochemical membrane[J]. Journal of Cleaner Production, 2023, 383: 135419.
[17] Ha H, Thompson R, Matteini P, et al. Effect of surface change by vacuum drying on the sedimentation stab ility of iron nanoparticles in volatile organic solvents [J]. Colloid and Interface Science Communications, 2 022, 48: 100625.
[18] Zhou Y, Wang T, Zhi D, et al. Applications of nanoscale zero-valent iron and its composites to the removal of antibiotics: a review [J]. Journal of Materials Science, 2019, 54(19): 12171-88.
[19] Lou Y, Cai Y, Tong Y, et al. Interaction between pollutants during the removal of polychlorinated biphenyl-heavy metal combined pollution by modified nanoscale zero-valent iron [J]. Science of The Total Environm ent, 2019, 673: 120-7.
[20] Katafias A, Lipińska M, Strutyński K. Alkaline hydrogen peroxide as a degradation agent of methylene blue—kinetic and mechanistic studies[J]. Reaction Kinetics, Mechanisms and Catalysis, 2010, 101(2): 251-266.
[21] Liu S P, Wang D Y, Wang M Y, et al. Effective degradation of Acid Orange 7 by alkali-catalyzed hydrogen pe roxide[J]. Journal of Huaqiao University (Natural Science), 2019, 40(2): 201-208.
[22] Qu M, Chen H, Wang Y, et al. Improved performance and applicability of copper-iron bimetal by sulfidatio n for Cr(VI) removal [J]. Chemosphere, 2021, 281: 130820.
[23] Huo X, Zhou P, Liu Y, et al. Removal of contaminants by activating peroxymonosulfate (PMS) using zero va lent iron (ZVI)-based bimetallic particles (ZVI/Cu, ZVI/Co, ZVI/Ni, and ZVI/Ag) [J]. RSC Advances, 2020, 10(4 7): 28232-42.

[24] Wang D Y, Zou J, Cai H H, et al. Effective degradation of Orange G and Rhodamine B by alkali-activated hy drogen peroxide: roles of HO-2 and O2·[J]. Environmental Science and Pollution Research International, 2 019, 26(2): 1445-1454.

[25] Peng H, Guo J, Li G, et al. Highly efficient oxidation of chromium (Ⅲ) with hydrogen peroxide in alkaline m edium[J]. Water Science and Technology, 2019, 79(2): 366-374.

[26] Zhu N, Ji H, Yu P, et al. Surface Modification of Magnetic Iron Oxide Nanoparticles [J]. Nanomaterials, 201 8, 8(10): 810.

[27] Wu Y, Guan C-Y, Griswold N, et al. Zero-valent iron-based technologies for removal of heavy metal(loid)s and organic pollutants from the aquatic environment: Recent advances and perspectives [J]. Journal of Cl eaner Production, 2020, 277: 123478.

[28] Lu H-J, Wang J-K, Ferguson S, et al. Mechanism, synthesis and modification of nano zerovalent iron in wat er treatment [J]. Nanoscale, 2016, 8(19): 9962-75.

[29] .

[30] Xu W, Hu X, Lou Y, et al. Effects of environmental factors on the removal of heavy metals by sulfide-modif ied nanoscale zerovalent iron [J]. Environmental Research, 2020, 187: 109662.

[31] Li L, Li Z, Song K, et al. Improving methane production from algal sludge based anaerobic digestion by co-p retreatment with ultrasound and zero-valent iron [J]. Journal of Cleaner Production, 2020, 255: 120214.

[32] Lai X, Ning X-a, He Y, et al. Treatment of a simulated sludge by ultrasonic zero-valent iron/EDTA/Air proce ss: Interferences of inorganic salts in polyaromatic hydrocarbon removal [J]. Waste Management, 2019, 8 5: 548-56.

[33] Fan K, Jin Z, Guo J, et al. Investigation on the surface layer formed during electrochemical modification of pure iron [J]. Applied Surface Science, 2019, 466: 466-71.

[34] Zhou G-N, Chen J-Q, Li W-Q, et al. Enhanced retention of surface-adsorbed atomic hydrogen through sulfi dation of nano zerovalent iron for water decontamination [J]. Chemical Engineering Journal, 2023, 474: 1 46248.

[35] Guan X, Yang H, Sun Y, et al. Enhanced immobilization of chromium(VI) in soil using sulfidated zero-valent iron [J]. Chemosphere, 2019, 228: 370-6.

[36] Guan X, Sun Y, Qin H, et al. The limitations of applying zero-valent iron technology in contaminants seque stration and the corresponding countermeasures: The development in zero-valent iron technology in the last two decades (1994–2014) [J]. Water Research, 2015, 75: 224-48.